Inactivation of *Caenorhabditis elegans* aminopeptidase DNPP-1 restores endocytic sorting and recycling in *tat-1* mutants

Xin Li[a,b], Baohui Chen[b], Sawako Yoshina[c], Tanxi Cai[d], Fuquan Yang[d], Shohei Mitani[c], and Xiaochen Wang[b]

[a]College of Biological Sciences, China Agricultural University, Beijing 100094, China; [b]National Institute of Biological Sciences, Beijing 102206, China; [c]Department of Physiology, School of Medicine and Institute for Integrated Medical Sciences, Tokyo Women's Medical University, Shinjuku-ku, Tokyo 162-8666, Japan; [d]Institute of Biophysics, Chinese Academy of Sciences, Beijing 100101, China

ABSTRACT In *Caenorhabditis elegans*, the P4-ATPase TAT-1 and its chaperone, the Cdc50 family protein CHAT-1, maintain membrane phosphatidylserine (PS) asymmetry, which is required for membrane tubulation during endocytic sorting and recycling. Loss of *tat-1* and *chat-1* disrupts endocytic sorting, leading to defects in both cargo recycling and degradation. In this study, we identified the *C. elegans* aspartyl aminopeptidase DNPP-1, loss of which suppresses the sorting and recycling defects in *tat-1* mutants without reversing the PS asymmetry defect. We found that tubular membrane structures containing recycling cargoes were restored in *dnpp-1 tat-1* double mutants and that these tubules overlap with RME-1–positive recycling endosomes. The restoration of the tubular structures in *dnpp-1 tat-1* mutants requires normal functions of RAB-5, RAB-10, and RME-1. In *tat-1* mutants, we observed alterations in membrane surface charge and targeting of positively charged proteins that were reversed by loss of *dnpp-1*. DNPP-1 displays a specific aspartyl aminopeptidase activity in vitro, and its enzymatic activity is required for its function in vivo. Our data reveal the involvement of an aminopeptidase in regulating endocytic sorting and recycling and suggest possible roles of peptide signaling and/or protein metabolism in these processes.

INTRODUCTION

Eukaryotic cells take up extracellular molecules by endocytosis. The consequent loss of plasma membrane constituents, such as lipids and receptors, is counterbalanced by endocytic recycling that returns most of the membrane components back to plasma membranes. Early endosomes are the sorting station in which receptor–ligand complexes are dissociated, due to the reduced pH of the

endosomal lumen (Harford *et al.*, 1983). Receptors are recycled back to plasma membranes through fast or slow recycling pathways (Grant and Donaldson, 2009), while ligands are transported to late endosomes and lysosomes for degradation (Mukherjee *et al.*, 1997). Early endosomes, whose functions require RAB5, phosphatidylinositol 3-phosphate (PI3P), and their effectors, employ both geometry- and motif-based mechanisms to sort cargoes according to their different destinations. Signaling receptors en route to lysosomes, such as EGFR (epidermal growth factor receptor), contain cytosolic domains that can be modified with mono-ubiquitination and subsequently recognized by the ESCRT (endosomal sorting complex required for transport) machinery and delivered to late endosomes and lysosomes (Maxfield and McGraw, 2004; Jovic *et al.*, 2010). In addition, sorting and recycling of some clathrin-independent cargoes may also involve positive selection processes (Grant and Donaldson, 2009). The geometry-based sorting mechanism, however, seems to be more frequently used in the sorting endosome to direct cargoes to plasma membranes or late endosomes/lysosomes (Maxfield and McGraw, 2004). This is mainly achieved through the pleiomorphic organization of sorting endosomes, which consist of

both thin tubules and large vesicles. The emanation and pinching-off of the thin tubules, which have a high surface area–to–volume ratio, efficiently sort membranes and membrane proteins away from soluble molecules that are retained and concentrated in the vesicular domain, which contains most of the endosome volume (Gruenberg, 2001). The tubular membrane structures of sorting endosomes can deliver recycling cargoes directly back to plasma membranes (fast recycling) or mature into endocytic recycling compartments (ERC) from which recycling endosomes form and carry cargoes back to plasma membranes (slow recycling; Maxfield and McGraw, 2004; Grant and Donaldson, 2009).

Rab GTPases and EHD (Eps15 homology domain) proteins are key regulators of endocytic sorting and recycling. RAB4 associates with both sorting endosomes and ERC and plays important roles in directing cargo recycling from early/sorting endosomes to plasma membranes (Jovic et al., 2010). RAB11 localizes to the ERC and trans-Golgi network (TGN) and is required for transporting cargo from the sorting endosome to the ERC and from the ERC to the plasma membrane. The EHD/RME-1 ATPases regulate cargo recycling in both mammals (EHD) and Caenorhabditis elegans (RME-1). The four mammalian EHD proteins are found to act at overlapping or distinct steps to direct cargo sorting and recycling (Grant and Caplan, 2008). Two Rab effectors have been identified as EHD-interacting proteins, suggesting a possible coordination between EHDs and Rabs (Grant and Donaldson, 2009). Recent structural studies suggest that EHD/RME-1 proteins may function similarly to dynamin to promote membrane fission for generating and releasing recycling cargo carriers (Daumke et al., 2007). In C. elegans, the sole EHD family protein, RME-1, localizes to tubulovesicular recycling endosomes in the basolateral membrane area of the intestine (Grant et al., 2001; Chen et al., 2006). Like mammalian EHDs, RME-1 tubulates liposomes in vitro and may act with the Bin Amphiphysin Rvs (BAR) domain–containing protein AMPH-1 to generate cargo carriers from recycling endosomes and deliver them to the cell surface (Pant et al., 2009). C. elegans and mammalian Rab GTPase 10 are key regulators of sorting and recycling, especially in the basolateral pathway of polarized epithelial cells (Babbey et al., 2006; Chen et al., 2006; Sano et al., 2007). C. elegans RAB-10 acts upstream of RME-1 to regulate the transport from early endosomes to ERC/recycling endosomes in intestinal cells (Chen et al., 2006). A RAB-10 to ARF-6 regulatory loop has recently been reported in which RAB-10 recruits CNT-1, the GTPase-activating protein (GAP) of ARF-6, as the effector, thus negatively regulating ARF-6 activity and causing reduced endosomal phosphatidylinositol-4,5-bisphosphate (PI(4,5)P2) (Shi et al., 2012). In addition to the positive regulators, C. elegans NUM-1 was found to negatively regulate endocytic recycling, probably by binding to and inhibiting the type IV P-type ATPase (P4-ATPase) TAT-1 (Nilsson et al., 2008, 2011).

Although organelle geometry has been suggested as playing a predominant role in separating cargoes in the sorting endosomes, little is known about how endosomal membranes are shaped into such different structures. Our previous studies showed that membrane phosphatidylserine (PS) asymmetry maintained by the P4-ATPase TAT-1 and its chaperone CHAT-1 plays important roles in forming and/or maintaining tubular membrane structures in sorting and recycling compartments. Loss of tat-1 and chat-1 function disrupts PS asymmetry across plasma and endosomal membranes and abrogates the tubular membrane structures, causing accumulation of recycling cargoes in aggregated early endosomes (Chen et al., 2010). However, as the aminophospholipid transporter that catalyzes PS translocation, TAT-1/CHAT-1 is unlikely to be the sole regulator of this process. In the present study, we report the identification and characterization of the M18 aminopeptidase DNPP-1, the loss of function of which

suppresses endocytic sorting and recycling but not cargo degradation defects in tat-1 mutants. We show that membrane surface charge is altered in tat-1 mutants but is largely restored in dnpp-1 tat-1 double mutants. Our data suggest that DNPP-1 acts as an aspartyl aminopeptidase to regulate endocytic transport in C. elegans.

RESULTS

Loss of dnpp-1 suppresses intestinal vacuolation of tat-1

C. elegans P4-ATPase TAT-1 and its chaperone, the Cdc50 family protein CHAT-1, maintain membrane PS asymmetry and regulate endocytic transport (Darland-Ransom et al., 2008; Ruaud et al., 2009; Chen et al., 2010). tat-1 and chat-1 mutants accumulate many large intestinal vacuoles, which are hybrid vesicles derived from early, late, and recycling endosomes, as well as lysosomes (Ruaud et al., 2009; Chen et al., 2010). To further investigate how TAT-1/CHAT-1 regulates endocytic sorting/recycling and to identify more regulators involved in this process, we performed a genetic screen to look for mutations that suppress the intestinal vacuolation of tat-1. From such a screen, we isolated a recessive mutation qx49, which completely suppressed intestinal vacuolation of tat-1(qx30) (Figure 1, A–C, and Supplemental Table S1). qx49 also suppresses the vacuolation phenotype in tat-1(tm3110) and chat-1(qx36) intestines (Supplemental Figure S1, A–D, and Table S1). qx49 mutants contain fewer and smaller gut granules than in wild type, a phenotype that was also observed in qx49 tat-1(qx30) double mutants (Figure 1, A, C, and D). Loss of rab-10, rme-1, or lmp-1 causes accumulation of large intestinal vacuoles that represent enlarged early endosomes, recycling endosomes, and lysosomes, respectively (Kostich et al., 2000; Grant et al., 2001; Chen et al., 2006). The qx49 mutation did not suppress intestinal vacuolation in rab-10, rme-1, or lmp-1 mutants, suggesting a specific effect on vacuoles caused by loss of tat-1/chat-1 function (Figure S1, I–N).

We cloned the gene affected in qx49 and found that it encodes the C. elegans homologue of mammalian aspartyl aminopeptidase (DAP), DNPP-1 (Figure S2). DAP is a widely distributed cytosolic enzyme that removes amino-terminal acidic amino acids from peptides. Sequencing of dnpp-1 in qx49 mutants revealed a G-to-A transition that resulted in replacement of Glu-331 by Lys, a residue conserved in both mouse and human homologues (Figure S2). A deletion mutant of dnpp-1, tm4588, or inactivation of dnpp-1 by RNA interference (RNAi) suppressed intestinal vacuoles in tat-1(qx30) mutants in a manner similar to qx49, suggesting that qx49 is likely a strong loss-of-function allele of dnpp-1 (Figure S1, E–H, and Table S1).

To examine where DNPP-1 is expressed, we generated a DNPP-1::mCHERRY translational fusion under control of the dnpp-1 promoter (P_{dnpp-1}DNPP-1::mCHERRY) that fully rescued the dnpp-1(qx49) phenotype (Figures 2, F and G, and S2A). DNPP-1 is expressed from early embryonic stages throughout larval and adult stages in various cell types, including muscle and intestine cells (Figure 2, A–E). Aspartyl aminopeptidases are cytosolic enzymes and, consistent with this, we found that DNPP-1::mCHERRY is diffuse in the cytosol of the intestine (Figure 2D; Kelly et al., 1983; Wilk et al., 1998, 2002). Expression of DNPP-1 driven by the intestine-specific vha-6 promoter but not the muscle-specific myo-3 promoter rescued the qx49 phenotype, indicating that DNPP-1 acts in a cell-autonomous manner to regulate the membrane trafficking process (Figure 2, I and J).

Loss of dnpp-1 does not reverse defective membrane PS asymmetry in tat-1 mutants

PS is confined to the cytosolic leaflet of plasma membranes and endomembranes but appears in both membrane leaflets when
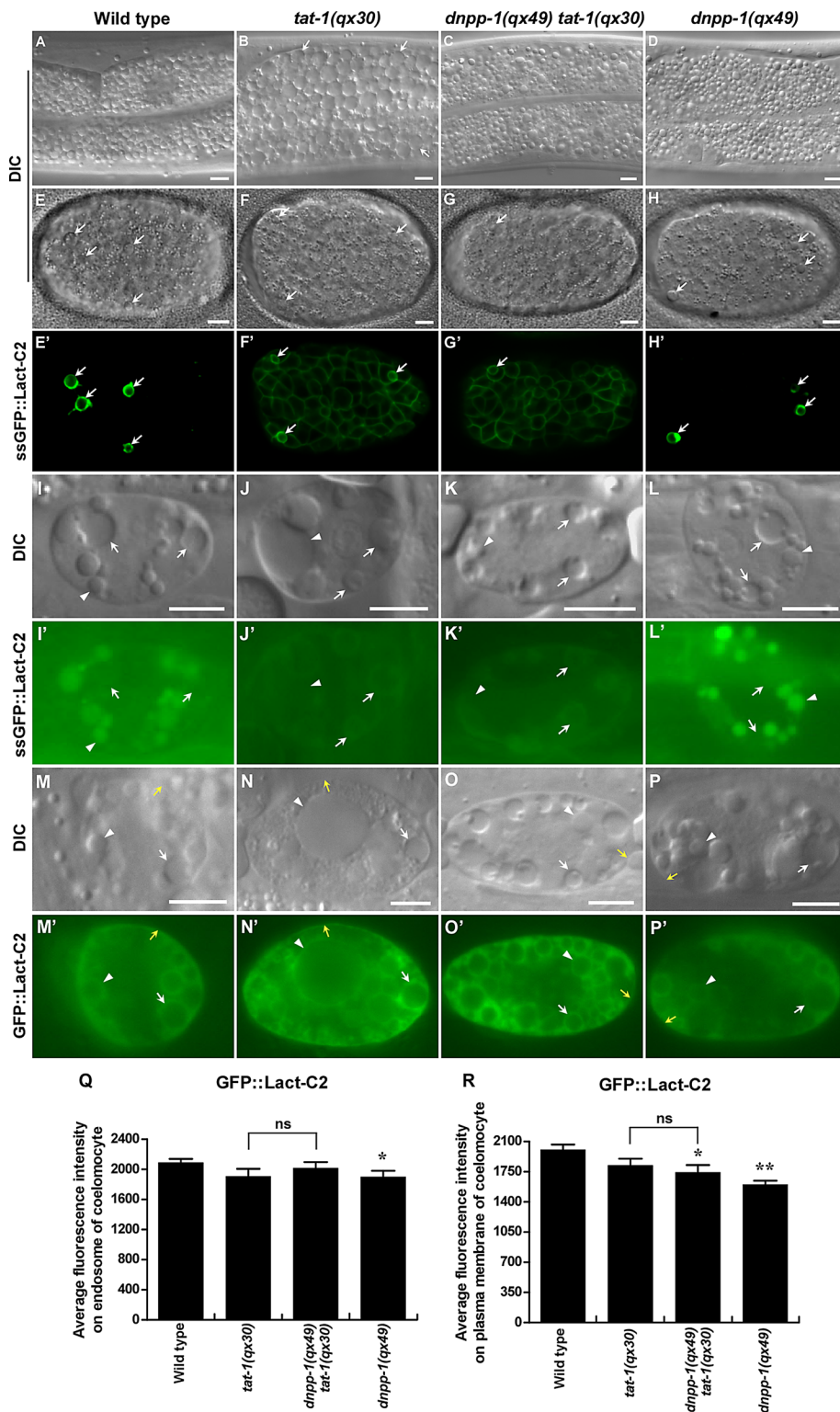
FIGURE 1: *dnpp-1(qx49)* suppresses the intestinal vacuolation of *tat-1(qx30)* mutants without reversing the PS asymmetry defect. (A–D) DIC images of the intestine in wild type (A), *tat-1(qx30)* (B), *dnpp-1(qx49) tat-1(qx30)* (C), and *dnpp-1(qx49)* (D). Abnormal vacuoles are indicated by arrows. (E–P') DIC and confocal fluorescent images of embryos (E–H') or coelomocytes (I–P') in wild type (E, E', I, I', M, M'), *tat-1(qx30)* (F, F', J, J', N, N'), *dnpp-1(qx49) tat-1(qx30)* (G, G', K, K', O, O'), and *dnpp-1(qx49)* (H, H', L, L', P, P') expressing ssGFP::Lact-C2 (P$_{hsp}$ssGFP::Lact-C2 in E–H') or GFP::Lact-C2 (P$_{unc-122}$GFP::Lact-C2 in M–P') or taking up and transporting ssGFP::Lact-C2 (P$_{myo-3}$ssGFP::Lact-C2 in I–L'). White arrows indicate cell corpses (E–H') and endosomes (I–P'); white arrowheads point to lysosomes (I–P'), and yellow arrows indicate plasma membranes (M–P'). Internalized GFP::Lact-C2 is absent from endosomes in

TAT-1 and CHAT-1 are lost (Chen *et al.*, 2010; Figure 1, E–F' and I–J'). To determine whether loss of *dnpp-1* suppresses PS appearance in the outer leaflet of plasma membranes in *tat-1* mutants, we expressed the secreted PS biosensor green fluorescent protein (GFP)::Lact-C2 (ssGFP::Lact-C2), which detects cell surface–exposed PS, and examined its pattern in wild type and *tat-1* and *dnpp-1* single mutants, and *dnpp-1 tat-1* double mutants. We found that GFP::Lact-C2 stained virtually all cells in *dnpp-1(qx49) tat-1(qx30)* double mutants as in *tat-1(qx30)* embryos, while cell surface–exposed PS was only observed on apoptotic cells in wild type (Figure 1, E–G'). These data suggest that plasma membrane PS asymmetry is still defective in *dnpp-1 tat-1* double mutants. To determine whether the *dnpp-1* mutation suppresses PS appearance in the luminal side of endomembranes in *tat-1* mutants, we examined the ssGFP::Lact-C2 pattern in coelomocytes, which are macrophage-like scavenger cells containing large endocytic vesicles (Chen *et al.*, 2010). Luminal PS is detected by ssGFP::Lact-C2 (P$_{myo-3}$ssGFP::Lact-C2), which after secretion from body wall muscle cells is taken up by coelomocytes through endocytosis and transferred to lysosomes via endocytic transport. We found that the internalized GFP::Lact-C2 was absent from endosomes in wild type, but labeled endosome membranes with a ring-like staining pattern in both *dnpp-1 tat-1* double mutants and *tat-1(qx30)* worms, indicating that loss of *dnpp-1* failed to suppress PS appearance in the luminal leaflet of endomembranes in *tat-1* mutants (Figure 1, I–K'). To investigate whether *dnpp-1* mutation causes changes in PS associated with the cytosolic leaflet, we expressed the PS biosensor GFP::Lact-C2 in coelomocytes (P$_{unc-122}$GFP::Lact-C2). The GFP signal was detected in the cytosolic leaflet of plasma membranes and the surfaces of endosomes

wild type and *dnpp-1(qx49)* single mutants but labels endomembranes in *tat-1(qx30)* single and *dnpp-1(qx49) tat-1(qx30)* double mutants. Scale bars: 5 μm. (Q and R) Quantification of average GFP::Lact-C2 intensity on endosomes (Q) and plasma membranes (R) in coelomocytes as shown in M–P'. Data are shown as mean ± SEM. Data derived from different mutant strains were compared with that from wild type. **, $p < 1.0 \times 10^{-5}$; *, $p < 0.05$; all other points had $p > 0.05$. Data derived from *dnpp-1(qx49) tat-1(qx30)* were also compared with those from *tat-1(qx30)*, and ns indicates that data are not significantly different.
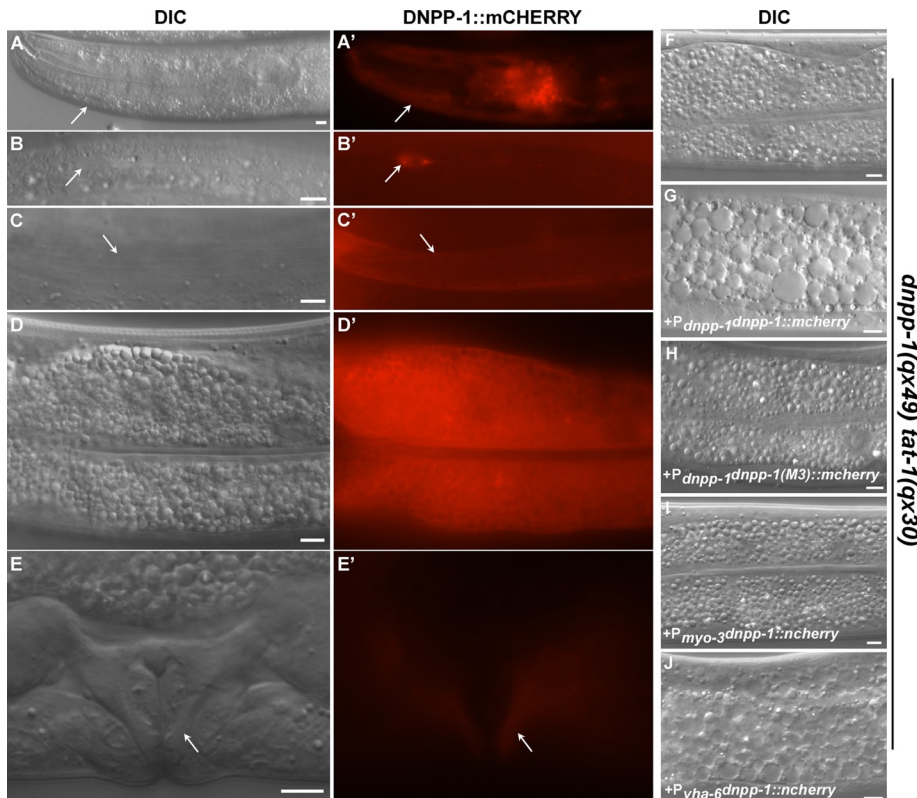
| DIC | DNPP-1::mCHERRY | DIC |

FIGURE 2: DNPP-1 is widely distributed and functions in a cell-autonomous manner. (A–E') DIC and fluorescent images of wild-type animals expressing DNPP-1::mCHERRY driven by the *dnpp-1* promoter. DNPP-1 expression was observed in various cell types (arrows), including pharynx (A, A'), neuron (B, B'), body wall muscle (C, C'), intestine (D, D'), and vulva (E, E'). (F–J) DIC images of the intestine in *dnpp-1(qx49) tat-1(qx30)* double mutants without (F) or with expression of DNPP-1::mCHERRY driven by the *dnpp-1* promoter (G), the intestine-specific promoter *vha-6* (J), the body wall muscle–specific promoter *myo-3* (I), or a mutant form of *dnpp-1* driven by the *dnpp-1* promoter (H). The suppression phenotype was reversed by expressing wild-type *dnpp-1* in intestine (J) but not body wall muscle cells (I) or a mutant form of DNPP-1 in which the critical zinc-binding residues were mutated (H). Scale bars: 5 µm.

and RAB-7 colocalized to only a limited number of small punctate structures, as in wild type (Figure 4, A–E). Similarly, the overlap of RAB-10, which localizes to the Golgi and early and recycling endosomes, and RME-1, which associates with basolateral recycling endosomes, on cytosolic aggregated vesicles in *tat-1* mutants was completely suppressed by *dnpp-1(qx49)* (Figure 4, F–J). In *dnpp-1(qx49) tat-1(qx30)* double mutants, RAB-10 and RME-1 labeled distinct vesicles, as in wild type (Figure 4, F–J; Grant et al., 2001; Chen et al., 2006). These data suggest that endocytic compartments along the sorting and recycling pathway are largely restored in *dnpp-1 tat-1* double mutants. Although RME-1 aggregation in the cytosol was suppressed by *dnpp-1* mutation, we observed reduced numbers of RME-1–positive puncta along basolateral membranes in *dnpp-1(qx49) tat-1(qx30)* double mutants, as in *tat-1(qx30)* single mutants, indicating defective RME-1–positive recycling endosomes in the basolateral membrane area (Figure 3, K and P). Consistent with this, we found that *dnpp-1(qx49)* single mutants contained slightly reduced basolateral RME-1–positive puncta, suggesting that loss of *dnpp-1* may affect RME-1–positive recycling endosomes (Figure 3, L (arrowheads) and P).

Loss of DNPP-1 suppresses cargo recycling defects in *tat-1* and *chat-1* mutants

Loss of *tat-1/chat-1* function disrupts endocytic transport from early to recycling endosomes, causing accumulation of recycling cargoes in abnormal early endosomes (Chen et al., 2010). We examined recycling of the human transferrin receptor (hTfR::GFP), the α-chain of the human interleukin-2 receptor TAC (hTAC::GFP), and the *C. elegans* glucose transporter 1 (GLUT-1::GFP), and found that all three cargoes accumulated in the cytosol of *tat-1* or *chat-1* intestines but mainly associated with plasma membranes in *dnpp-1 tat-1* double mutants, as in wild type (Figures 5, A–O, and S3, E–H). This indicates that the abnormal distribution of the recycling markers in *tat-1* and *chat-1* mutants is reversed by *dnpp-1* mutation. Loss of *dnpp-1* alone did not affect the distribution of hTfR, a clathrin-dependent cargo, but caused mild accumulation of hTAC and GLUT-1, which are internalized in a clathrin-independent manner (Figure 5, N and O). The suppression of abnormal cargo distribution in *dnpp-1(qx49) tat-1(qx30)* was reversed by DNPP-1 expression, confirming that it was indeed caused by loss of *dnpp-1* function (Figure S3, K–N).

The P4-ATPase TAT-1 and its chaperone, CHAT-1, localize to tubular membrane structures of sorting and recycling compartments and are required for forming and/or maintaining the tubular extensions, thus promoting cargo sorting and recycling (Chen et al., 2010). The recycling cargoes GLUT-1::GFP and hTAC::GFP labeled tubular membrane structures that overlapped with RME-1–positive recycling endosomes, indicating normal cargo recycling in wild type (Chen et al., 2010; Figure 5, P–P''). In *tat-1(qx30)* mutants,

and lysosomes, with a similar intensity observed in wild type, *tat-1*, and *dnpp-1 tat-1*, suggesting that loss of *dnpp-1* does not obviously change the PS level in the cytosolic leaflet of membranes in *tat-1* mutants (Figure 1, M–R; Chen et al., 2010). In *dnpp-1(qx49)* single mutants, PS was not observed on the cell surface or in the luminal leaflet of endomembranes, while the PS level in the cytosolic leaflet of plasma and endomembranes was slightly lower than in wild type (Figure 1, H, H', L, L', and P–R). These data suggest that the asymmetric distribution of PS across plasma membranes or endomembranes is not affected by *dnpp-1* mutation, and loss of *dnpp-1* fails to suppress the PS asymmetry defect in *tat-1* mutant.

dnpp-1(qx49) mutants suppress aggregation of endosomes in *tat-1(qx30)* mutants

In *tat-1* and *chat-1* mutants, endocytic transport from early to recycling or late endosomes is disrupted, causing aggregation of early, recycling, and late endosomes (Chen et al., 2010). We found that loss of DNPP-1 did not affect RAB-5– or RAB-10–positive puncta but significantly suppressed aggregation of RAB-5–, RAB-7–, RAB-10–, or RME-1–positive vesicles in *tat-1* or *chat-1* mutants (Figures 3, 7, A–D and I, and S3, A–D). In *tat-1(qx30)* mutants, RAB-5, which marks early endosomes, and RAB-7, which mainly marks late endosomes and early lysosomes, overlapped on aggregated cytosolic vesicles, but in *dnpp-1(qx49) tat-1(qx30)* double mutants, RAB-5
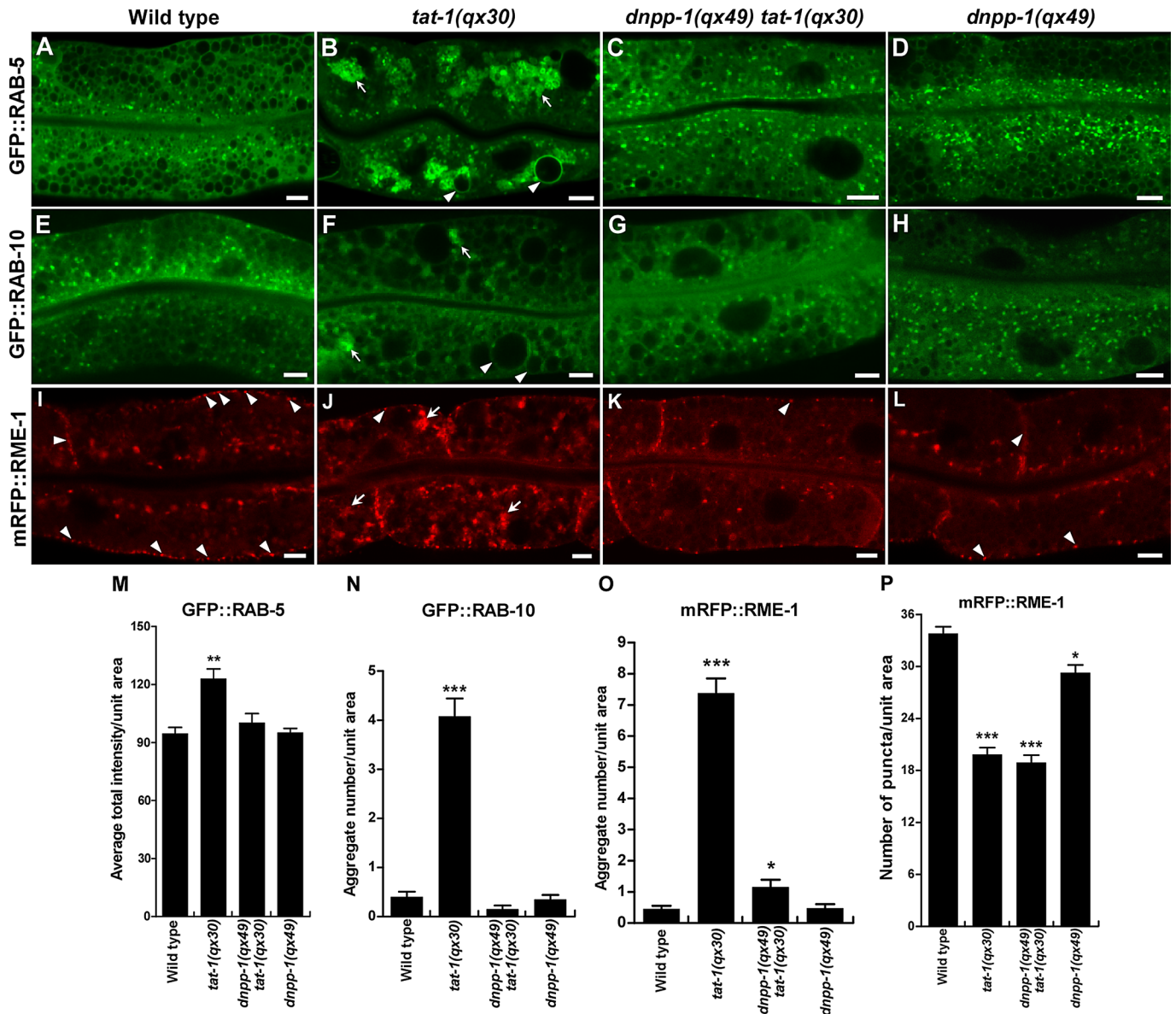
FIGURE 3: Loss of *dnpp-1* suppresses the aggregation of endosomes in *tat-1(qx30)* mutants. Confocal fluorescent images of the intestine in wild type (A, E, I), *tat-1(qx30)* (B, F, J), *dnpp-1(qx49) tat-1(qx30)* (C, G, K), and *dnpp-1(qx49)* (D, H, L) expressing GFP::RAB-5 (A–D), GFP::RAB-10 (E–H), or mRFP::RME-1 (I–L). Arrows indicate aggregated vesicles in the cytoplasm, and arrowheads point to abnormal vacuoles (B, F) or RME-1–positive vesicles in close proximity to the basolateral membranes (I–L). More RME-1 puncta along the basolateral membrane were observed in wild type (I, arrowheads) than in *dnpp-1(qx49)* (L, arrowheads). Quantifications are shown in (M–P). Data are shown as mean ± SEM. ***, $p < 1.0 \times 10^{-10}$; **, $p < 1.0 \times 10^{-5}$; *, $p < 0.05$. Scale bars: 5 μm.

hTAC::GFP-positive tubular structures were abrogated, and hTAC::GFP was absent from RME-1–positive recycling endosomes (Figure 5, Q–Q''). We found that tubular membrane structures containing hTAC::GFP were restored in *dnpp-1(qx49) tat-1(qx30)* double mutants or *dnpp-1(qx49);chat-1(RNAi)* animals, and the majority of hTAC::GFP colocalized with mRFP::RME-1–positive recycling endosomes (Figures 5, R–R'', and S3, I and J). The hTAC::GFP-positive tubules in *dnpp-1(qx49) tat-1(qx30)* double mutants were disrupted when DNPP-1 was expressed, indicating that inactivation of DNPP-1 is required for the restoration of cargo-containing tubular extensions in *tat-1* mutants (Figure S3, M and N). We found that hTAC::GFP-positive tubules were still present in *dnpp-1(qx49) tat-1(qx30);lmp-1(RNAi)* worms, which contained many intestinal

vacuoles, due to inactivation of *lmp-1* (Figure S3, Q–T). This suggests that the tubular membrane structures are indeed absent in *tat-1* mutants rather than simply being hidden by vacuoles.

In the *C. elegans* intestine, RAB-5, RAB-10, and RME-1 act at different steps to regulate cargo sorting and recycling. RAB-5 maintains sorting endosome function; RAB-10 regulates cargo transport from sorting to recycling endosomes; and RME-1 acts downstream of RAB-10 to promote cargo recycling to plasma membranes. We found that the restoration of cargo recycling in *dnpp-1(qx49) tat-1(qx30)* double mutants was abrogated when *rab-5* or *rab-10* was inactivated by RNAi (Figures 6, A–C and E, and S3, U–W and Y). The hTAC::GFP-positive tubules, which are restored in *dnpp-1 tat-1* double mutants, became aggregated or diffuse when *rab-5* or *rab-10*
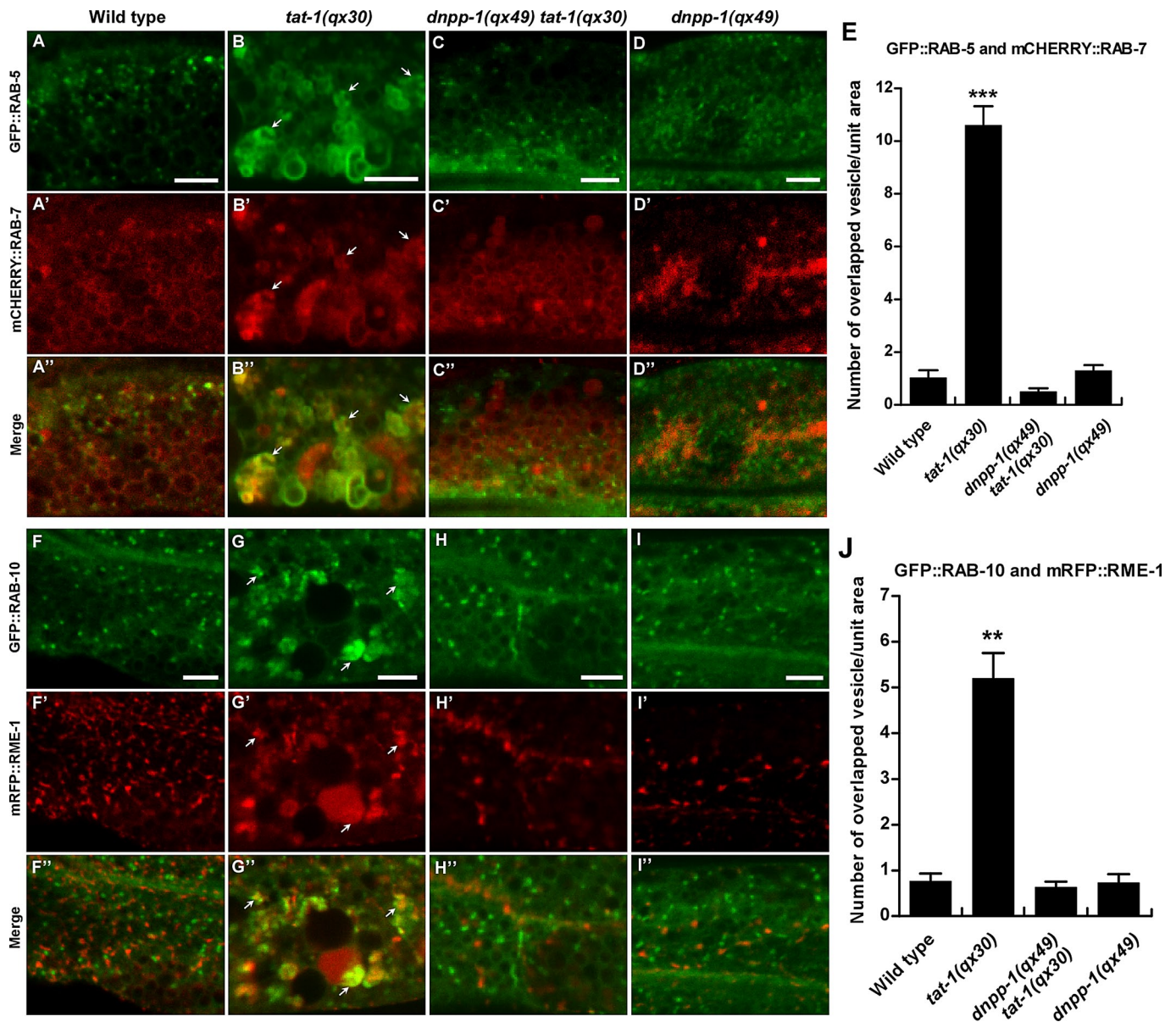
FIGURE 4: The abnormal sorting endosome phenotype is suppressed in *dnpp-1(qx49) tat-1(qx30)* double mutants. Confocal fluorescent images of the intestine in wild type (A–A″, F–F″), *tat-1(qx30)* (B–B″, G–G″), *dnpp-1(qx49) tat-1(qx30)* (C–C″, H–H″), and *dnpp-1(qx49)* (D–D″, I–I″) coexpressing GFP::RAB-5 and mCHERRY::RAB-7 (A–D″) or GFP::RAB-10 and mRFP::RME-1 (F–I″). Arrows indicate aggregated vesicles positive for both RAB-5 and RAB-7 or RME-1 and RAB-10. Quantification of the colocalization is shown in (E) and (J). Data are shown as mean ± SEM. ***, $p < 1.0 \times 10^{-10}$; **, $p < 1.0 \times 10^{-5}$. Scale bars: 5 μm.

was lost (Figure 6, F–N). We found that loss of *rme-1* also disrupted cargo recycling in *dnpp-1 tat-1* double mutants. hTAC::GFP accumulated as ring-like or punctate but not tubular structures in the basolateral membrane area, consistent with the role of RME-1 in generating and transporting cargo carriers to plasma membranes (Figures 6, D and E and O–Q, and S3, X and Y). Therefore the restoration of cargo recycling in *tat-1* mutants by inactivation of DNPP-1 requires RAB-5, RAB-10, and RME-1 function along the sorting and recycling pathway.

Cargo degradation remains defective in *dnpp-1(qx49) tat-1(qx30)*

In addition to disrupting cargo recycling, loss of *tat-1* and *chat-1* also affects the degradation pathway, as indicated by accumulation

of yolk protein (VIT-2::GFP) in both embryos and intestinal cells of aged adult animals (Chen *et al.*, 2010; Figures 7, J–Q and Z1, and S4, A–B′ and E). In contrast to the well-suppressed cargo recycling defects, we found that loss of *dnpp-1* enhanced the cargo degradation phenotype in *tat-1(qx30)* mutants, with further delayed VIT-2::GFP degradation during embryogenesis and in aged adult worms (Figures 7, R–U and Z1, and S4, C, C′ and E).

We examined late endosomes and lysosomes in *dnpp-1(qx49)* and *dnpp-1(qx49) tat-1(qx30)* double mutants. The abnormal aggregation of GFP::RAB-7 in *tat-1(qx30)* was greatly suppressed by *dnpp-1(qx49)*, although severe aggregation of GFP::RAB-7 was seen in *dnpp-1(qx49)* single mutants (Figure 7, A–D and I). Both *tat-1* single and *dnpp-1 tat-1* double mutants contained fewer and smaller Lysotracker Red–positive lysosomes (Figure 7, E–G and
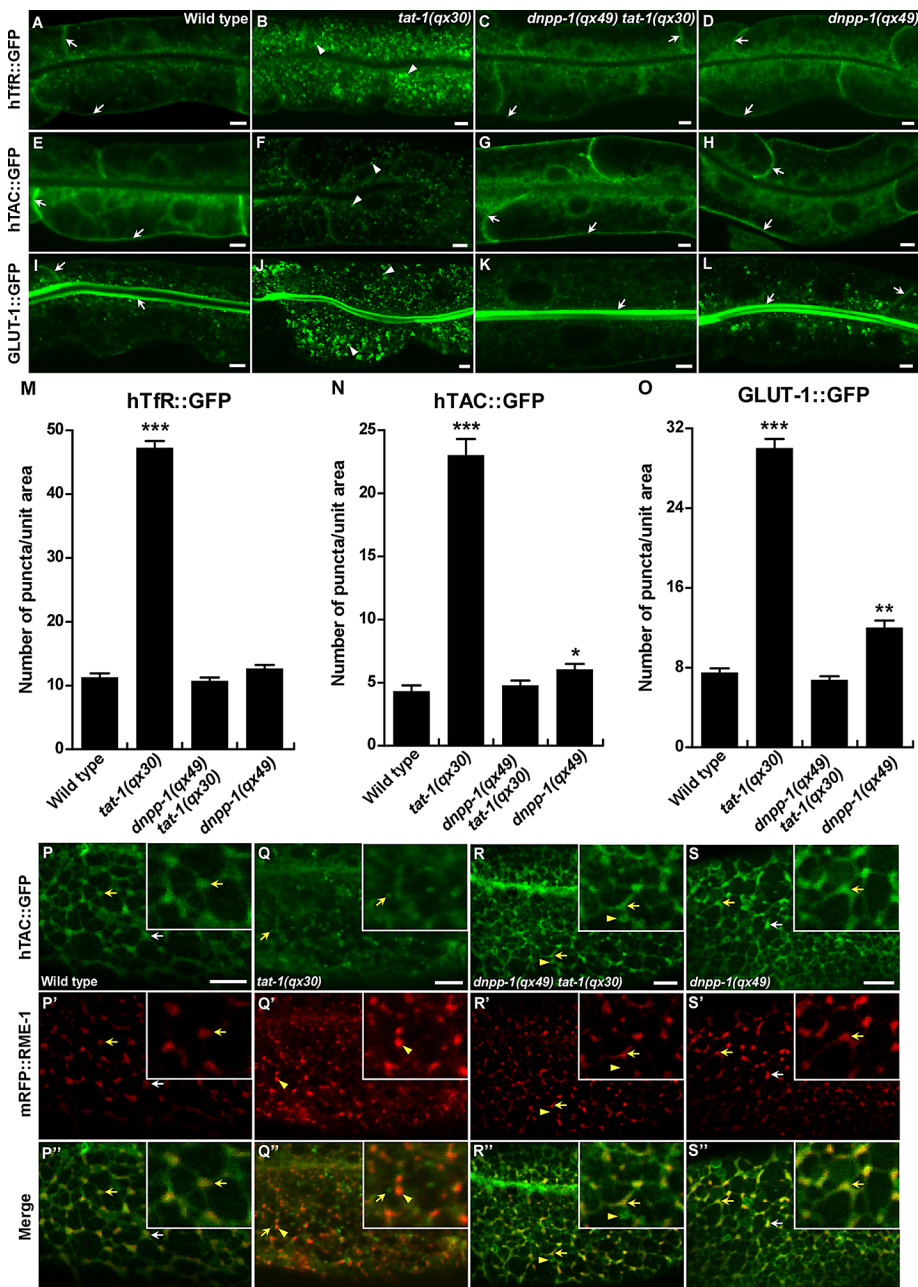
FIGURE 5: Cargo recycling defects in *tat-1(qx30)* are suppressed by *dnpp-1(qx49)*. (A–L) Confocal fluorescent images of the intestine in wild type (A, E, I), *tat-1(qx30)* (B, F, J), *dnpp-1(qx49) tat-1(qx30)* (C, G, K), and *dnpp-1(qx49)* (D, H, L) expressing hTfR::GFP (A–D), hTAC::GFP (E–H), or GLUT-1::GFP (I–L). GFP signal was mainly seen on plasma membranes in wild type, *dnpp-1(qx49) tat-1(qx30)*, and *dnpp-1(qx49)* (arrows) but accumulated intracellularly in *tat-1(qx30)* mutants (arrowheads). (M–O) Quantification of the intracellular accumulation of hTfR::GFP (M), hTAC::GFP (N) and GLUT-1::GFP (O) as shown in (A–L). In (M–O), data are shown as mean numbers of labeled structures ± SEM. ***, $p < 1.0 \times 10^{-10}$; **, $p < 1.0 \times 10^{-5}$; *, $p < 0.05$. (P–S″) Confocal fluorescent images of the basolateral membrane area of the intestine (top focal plane) in wild type (P–P″), *tat-1(qx30)* (Q–Q″), *dnpp-1(qx49) tat-1(qx30)* (R–R″), and *dnpp-1(qx49)* (S–S″) coexpressing hTAC::GFP and mRFP::RME-1. hTAC and RME-1 overlapped on tubulovesicular structures (arrows) in wild type (P″), *dnpp-1(qx49) tat-1(qx30)* (R″) and *dnpp-1(qx49)* (S″), but were separated in *tat-1(qx30)* mutants (Q″, arrows and arrowheads indicate hTAC and RME-1 puncta, respectively). Some hTAC::GFP-positive structures in *dnpp-1(qx49) tat-1(qx30)* intestine lacked mRFP::RME-1 signal (R–R″, arrowheads). Insets show an amplified view with a 2× magnification of the structures indicated by yellow arrows or arrowheads. Scale bars: 5 μm.

Z). *dnpp-1(qx49)* single mutants only showed a mild defect in lysosome acidification, which is consistent with normal VIT-2::GFP degradation in both embryos and adult intestines (Figures 7, H and V–Z1, and S4, D–E). Collectively, these data indicate that loss of *dnpp-1* alone not only affects RAB-7–positive endosomes but also fails to reverse cargo degradation defects in *tat-1(qx30)*.

Surface charge and protein targeting are altered in *tat-1* mutants but restored by loss of *dnpp-1*

The inner surface of plasma membranes has been shown to be more negatively charged than membranes of endocytic compartments, most likely due to the unique accumulation of highly charged phosphoinositides PIP2, phosphatidylinositol 3,4,5-trisphosphate (PI(3,4,5)P3, PIP3) and the presence of abundant phosphatidylserine (McLaughlin and Murray, 2005; Yeung *et al.*, 2008). The negative surface charge directs targeting of positively charged proteins to different membrane compartments through electrostatic interactions (Heo *et al.*, 2006; Yeung *et al.*, 2008). We investigated whether surface charges are altered in *tat-1* mutants with defective membrane PS asymmetry by expressing a series of charge biosensors in the intestine (Roy *et al.*, 2000). We found that the most cationic biosensor (8+) strongly labeled the plasma membrane in wild-type intestine, whereas the least cationic biosensor (2+) mainly associated with membranes of intracellular vesicles (Figure 8, A and M). As the charge of the probes decreased, plasma membrane labeling gradually reduced, while staining of intracellular membranes increased (Figure 8, E and I). These results are consistent with previous observations in mammalian cells that plasma membranes are the most negatively charged membrane compartment (Yeung *et al.*, 2008). In *tat-1(qx30)* worms, however, the 8+ probe weakly labeled plasma membranes but strongly labeled large abnormal vacuoles, suggesting reduced negative charge in the inner leaflet of plasma membranes and/or increased negativity on the surfaces of abnormal vacuoles (Figure 8, B and U). The plasma membrane labeling by the 6+ and 4+ probes was also reduced in *tat-1(qx30)*, with a concomitant increase in cytoplasmic staining (Figure 8, F, J, V, and W) consistent with decreased negative surface charge of plasma membranes. The GFP::2+ probe was observed on vacuoles or in aggregates in *tat-1(qx30)* animals (Figure 8N). These data suggest that disruption of PS asymmetry affects membrane
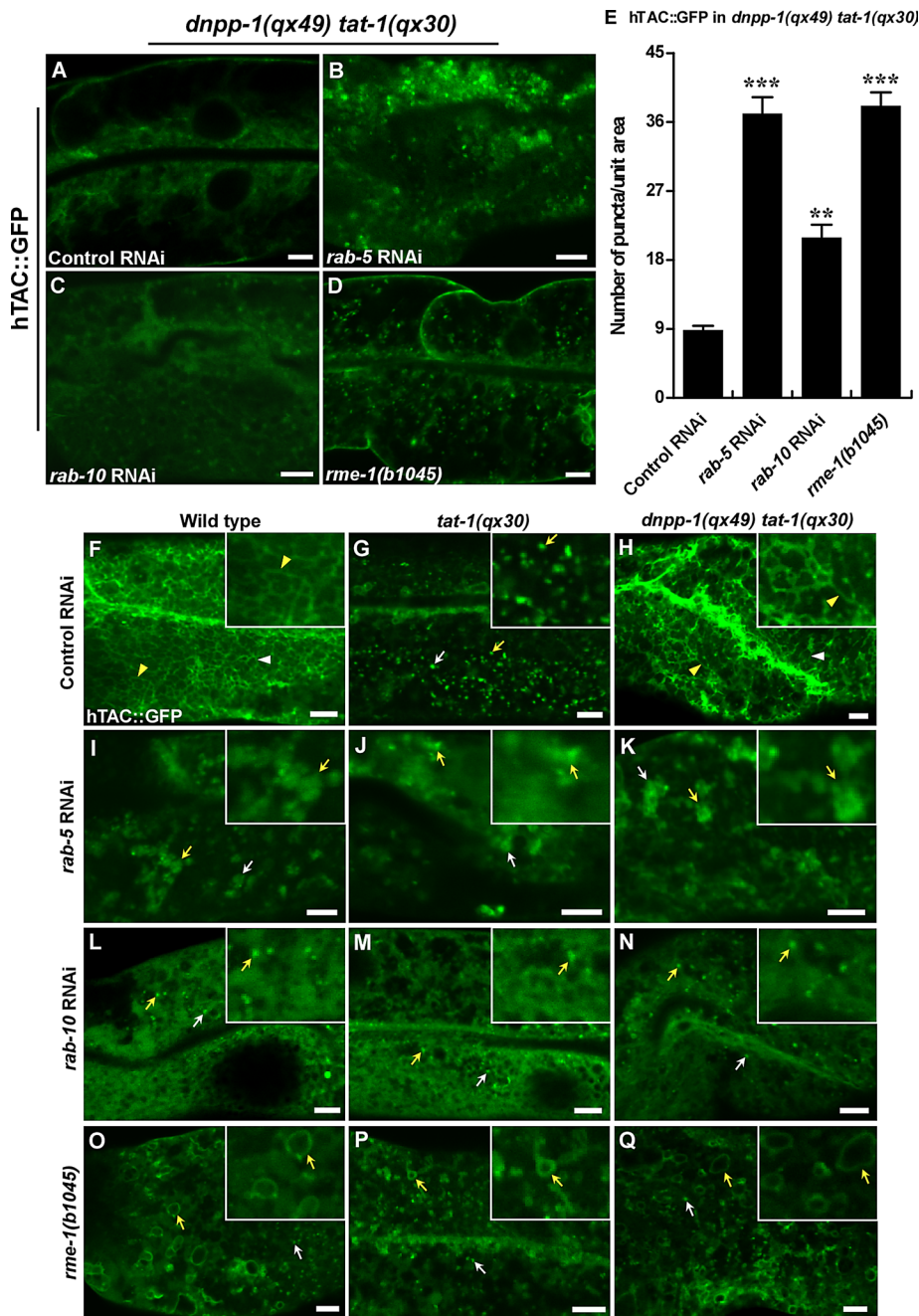
FIGURE 6: Restoration of cargo recycling in *tat-1(qx30)* by the *dnpp-1* mutation requires the functions of RAB-5, RAB-10, and RME-1. (A–D) Confocal fluorescent images of the intestine in *dnpp-1(qx49) tat-1(qx30)* mutants expressing hTAC::GFP and treated with control RNAi (A), *rab-5* RNAi (B), *rab-10* RNAi (C), or carrying a *rme-1* mutation (D). Quantification of the intracellular accumulation of hTAC::GFP is shown in (E). Data are shown as mean ± SEM. ***, $p < 1.0 \times 10^{-10}$; **, $p < 1.0 \times 10^{-5}$. (F–Q) Confocal fluorescent images of the basolateral membrane area of the intestine (top focal plane) in wild type (F, I, L, O), *tat-1(qx30)* (G, J, M, P), and *dnpp-1(qx49) tat-1(qx30)* (H, K, N, Q) expressing hTAC::GFP and treated with control RNAi (F–H), *rab-5* RNAi (I–K), *rab-10* RNAi (L–N) or carrying a *rme-1* mutation (O–Q). hTAC-positive tubules were observed in wild type and *dnpp-1(qx49) tat-1(qx30)* treated with control RNAi but were disrupted when *rab-5*, *rab-10*, or *rme-1* was inactivated. Arrowheads point to hTAC tubules, and arrows indicate hTAC-positive structures (puncta, aggregates, or rings) when tubules are disrupted. Insets show magnified (2×) views of the structures indicated by yellow arrows or arrowheads. Scale bars: 5 μm.

(Heo *et al.*, 2006; Yeung *et al.*, 2008). To determine whether alterations of surface charge in *tat-1* mutants affect membrane targeting of proteins bearing positive charges, we examined the localization of *C. elegans* RAS-2, which contains a C-terminal polybasic cluster bearing seven positive charges. GFP::RAS-2 strongly labeled plasma membranes and weakly stained membranes of intracellular vesicles in the wild-type intestine (Figure 8Q). In *tat-1(qx30)* animals, however, the plasma membrane localization of RAS-2 was significantly reduced, and GFP::RAS-2 became more evident on intracellular membranes, including those of abnormal vacuoles or aggregated vesicles within the cytoplasm (Figure 8, R and X). These data suggest that disrupted PS asymmetry in *tat-1* mutants alters membrane surface charges, leading to protein redistribution from plasma membranes to endomembranes and/or dissociation from both membranes.

We next examined whether altered surface charge and protein targeting can be reversed by *dnpp-1(lf)*, which restores the endocytic sorting and recycling in *tat-1(qx30)* animals. We found that the plasma membrane labeling by 8+, 6+, and 4+ probes dramatically increased in *dnpp-1(qx49) tat-1(qx30)* double mutants, while the cytoplasmic staining decreased (Figure 8, C, G, K, and U–W). Some internal structures that labeled strongly with GFP::8+ were still observed in *dnpp-1 tat-1* worms, suggesting incomplete reversion of membrane surface charge (Figure 8C). The *dnpp-1 tat-1* double mutants also showed significantly reduced GFP::2+ aggregation; GFP::2+ mainly associated with intracellular vesicles, as in wild type (Figure 8O). Consistent with this, we observed that RAS-2 mainly associated with plasma membranes in *dnpp-1(qx49) tat-1(qx30)* double mutants, as in wild type (Figure 8, S and X). No abnormal charge distribution or protein targeting was seen in *dnpp-1(qx49)* single mutants (Figure 8, D, H, L, P, T and U–X). The reversed plasma membrane targeting of GFP::RAS-2 in *dnpp-1(qx49) tat-1(qx30)* double mutants was disrupted by DNPP-1 expression, confirming that loss of DNPP-1 restores membrane surface charge and protein targeting in *tat-1* mutants (Figure S3, O and P).

DNPP-1 acts as an aspartyl aminopeptidase to regulate endocytic transport

dnpp-1 encodes a *C. elegans* homologue of aspartyl aminopeptidase. We determined the enzyme activity of DNPP-1 in vitro using recombinant DNPP-1 and various fluorogenic peptide substrates (McGowan *et al.*, 2009). We found

surface charge, causing redistribution and/or dissociation of cationic probes. Negatively charged membranes contribute to the targeting of proteins with polybasic clusters through electrostatic interactions
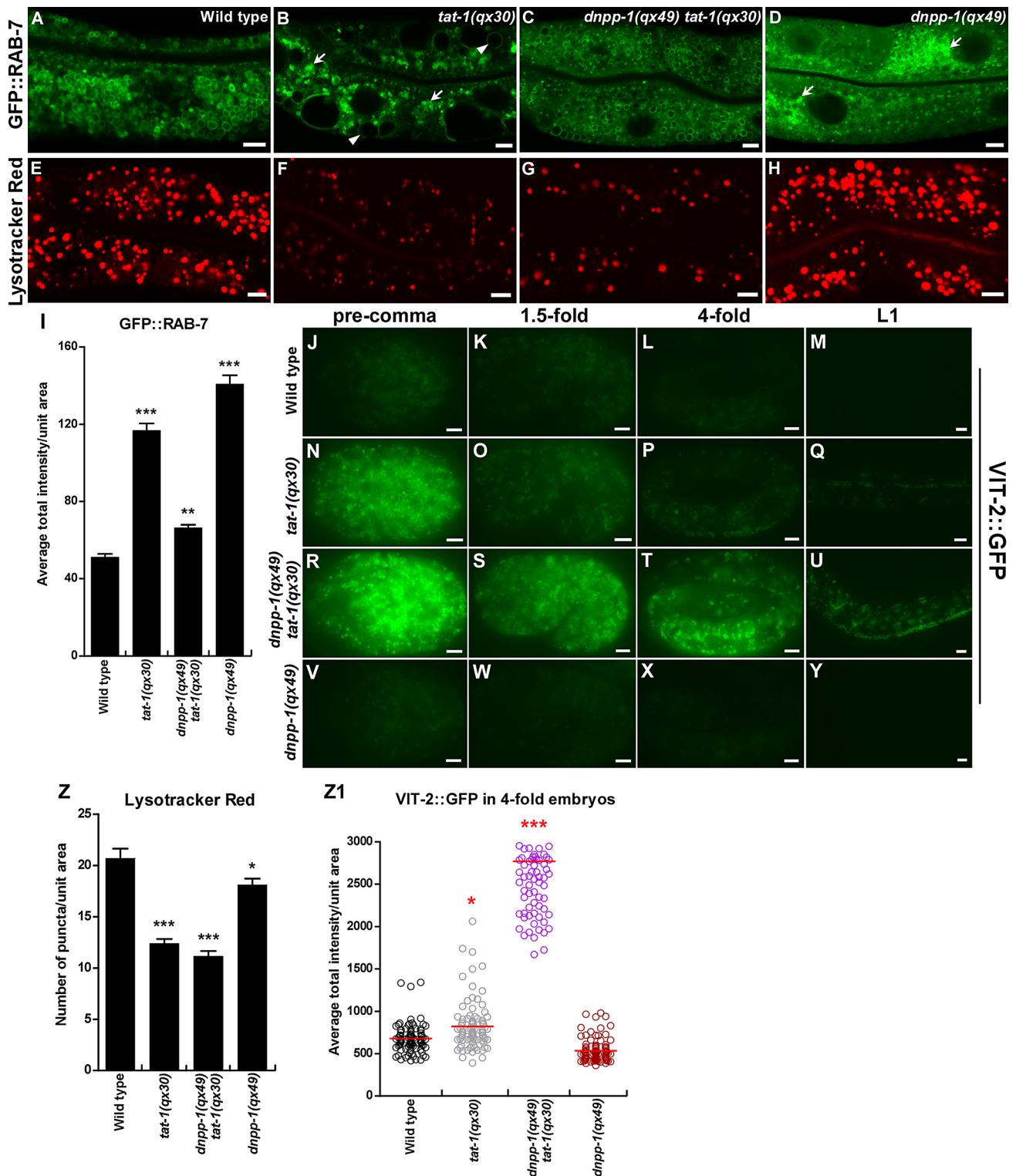
FIGURE 7: The cargo degradation defect in *tat-1(qx30)* is not suppressed by *dnpp-1(qx49)*. (A–H) Confocal fluorescent images of the intestine in wild type (A, E), *tat-1(qx30)* (B, F), *dnpp-1(qx49) tat-1(qx30)* (C, G), and *dnpp-1(qx49)* (D, H) expressing GFP::RAB-7 (A–D) or stained by Lysotracker Red (E–H). Arrowheads indicate abnormal vacuoles, and arrows show aggregated intracellular vesicles. Quantifications (mean ± SEM) are shown in (I) and (Z). (J–Y) Fluorescent images of wild type (J–M), *tat-1(qx30)* (N–Q), *dnpp-1(qx49) tat-1(qx30)* (R–U), and *dnpp-1(qx49)* (V–Y) embryos expressing the yolk reporter VIT-2::GFP. Quantification of yolk accumulation in fourfold-stage embryos is shown in (Z1). Red lines represent the average intensity of VIT-2::GFP in each strain. In (I, Z, Z1), ***, $p < 1.0 \times 10^{-10}$; **, $p < 1.0 \times 10^{-5}$; *, $p < 0.05$. Scale bars: 5 µm.

that DNPP-1 cleaved H-Asp-NHMec and H-Glu-NHMec, deriva-tives of the two acidic amino acids that are known substrates of aspartyl aminopeptidase, with k_{cat}/K_m values of 10,330.6 and

15,324.1 s^{-1}M^{-1}, respectively (Table 1). DNPP-1 did not show any activity toward other substrates, such as H-Leu-NHMec, H-Arg-NHMec, or H-Ala-NHMec (Table S2). Aspartyl aminopeptidases
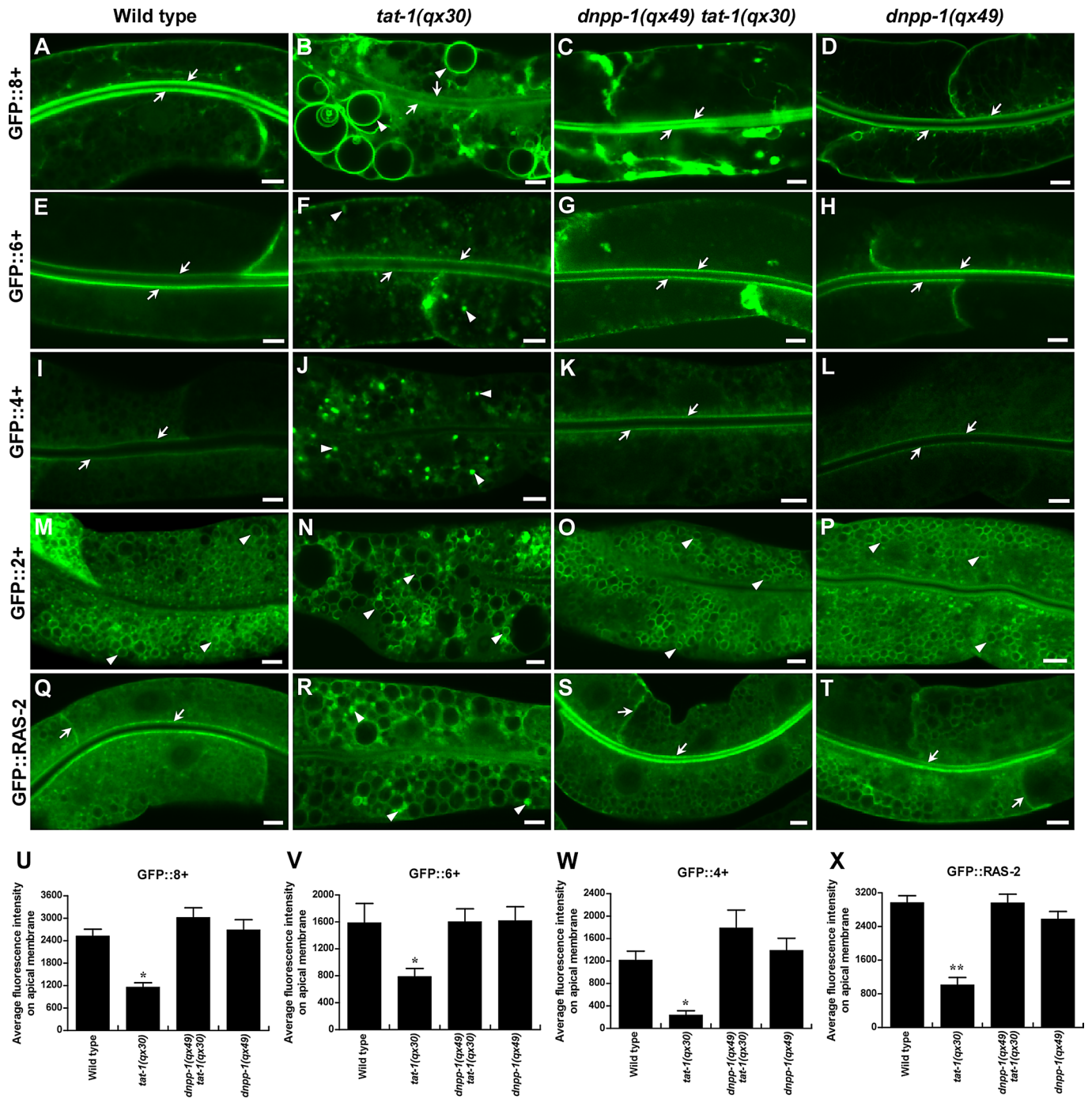
FIGURE 8: The altered membrane surface charge and protein targeting in *tat-1(qx30)* are reversed in *dnpp-1(qx49) tat-1(qx30)*. (A–T) Confocal fluorescent images of the intestine in wild type (A, E, I, M, Q), *tat-1(qx30)* (B, F, J, N, R), *dnpp-1(qx49) tat-1(qx30)* (C, G, K, O, S) and *dnpp-1(qx49)* (D, H, L, P, T) expressing GFP::8+ (A–D), GFP::6+ (E–H), GFP::4+ (I–L), GFP::2+ (M–P), or GFP::RAS-2 (Q–T). The cationic biosensors (8+, 6+, 4+) and the positively charged protein RAS-2 strongly labeled plasma membranes in wild type, *dnpp-1(qx49) tat-1(qx30)*, and *dnpp-1(qx49)* (arrows) but accumulated intracellularly in *tat-1(qx30)* animals (arrowheads). Quantifications are shown in panels (U–X). Data are shown as mean ± SEM. **, $p < 1.0 \times 10^{-5}$; *, $p < 0.05$; all other points had $p > 0.05$. Scale bars: 5 µm.

belong to the M18 family of metalloproteases, which contain three histidine residues involved in binding to cocatalytic zinc atoms. Mutations of these histidine residues cause complete loss of enzymatic activity (Wilk *et al.*, 2002). We found that DNPP-1(M3), in which the three conserved histidine residues were mutated to phenylalanine, and DNPP-1(E331K), the mutated version of DNPP-1 in the *qx49* allele, had no enzymatic activity, consistent with *qx49* being a strong loss-of-function allele of *dnpp-1* (Table 2 and Figure S2B). Two known metalloprotease inhibitors, EDTA and *o*-phenanthroline, significantly suppressed the enzymatic activity of DNPP-1 (Table 3). These data indicate that DNPP-1 is an aspartyl metallopeptidase. We found that

Substrate	K_m (10^{-3} mM)	k_{cat} (s^{-1})	k_{cat}/K_m (s^{-1} M^{-1})
H-Asp-NHMec	13.58	0.136	10,330.6
H-Glu-NHMec	8.854	0.134	15,324.1

Kinetic parameters were obtained at pH 7.5, as described in *Materials and Methods*. Each value represents the mean of two independent experiments.

TABLE 1: Kinetic parameters for the hydrolysis of H-Asp-NHMec and H-Glu-NHMec by DNPP-1.

	DNPP-1(WT)	DNPP-1(M3)	DNPP-1(E331K)
H-Asp-NHMec	100%	0.047%	0.018%
H-Glu-NHMec	100%	0.036%	0.034%

Enzymatic activity was measured as described in *Materials and Methods*. The aspartyl aminopeptidase activity of wild-type DNPP-1 was defined as 100%. Data shown are representative of two independent experiments.

TABLE 2: Aspartyl aminopeptidase activity of wild-type and mutant DNPP-1.

Inhibitor	Concentration (mM)	Activity (%)
—	—	100
EDTA	5	13.7
	20	11.0
	50	7.8
o-Phenanthroline	2.5	5.6
	5	2.2

The enzyme activity was measured using H-Asp-NHMec as a substrate. The enzymatic activity of DNPP-1 without treatment was defined as 100%. Data shown are representative of two independent experiments.

TABLE 3: Effect of inhibitors on aspartyl aminopeptidase activity of DNPP-1.

expression of the mutant DNPP-1 (DNPP-1(M3)::mCHERRY), which lacks the zinc-binding sites and has no enzymatic activity, failed to rescue the *dnpp-1(qx49) tat-1(qx30)* double mutant phenotype (Figures 2H and S2A), suggesting that DNPP-1 functions as an aspartyl aminopeptidase in vivo.

DISCUSSION
The P4-ATPase TAT-1 and its chaperone, CHAT-1, enrich PS in the cytosolic leaflet of plasma and endomembranes, thereby maintaining membrane PS asymmetry, which is required for forming and/or maintaining the tubular membrane structures of sorting and recycling compartments (Chen *et al.*, 2010). In agreement with the contribution of PS-to-membrane surface charge (Yeung *et al.*, 2008), we found that disruption of PS asymmetry by *tat-1* mutation led to redistribution of positively charged biosensors from plasma membranes to endomembranes or disassociation from both membranes. Moreover, alterations in membrane surface charge caused by defective PS asymmetry result in mistargeting of positively charged proteins. Thus, in addition to directly affecting membrane curvature, PS asymmetry controlled by TAT-1/CHAT-1 also contributes to the recruitment of regulatory proteins through PS-binding and electrostatic interactions (Sune and Bienvenue, 1988; McMahon and Gallop, 2005). In this study, we identified the *C. elegans* aspartyl aminopeptidase DNPP-1, loss of function of which restores sorting

endosomes and cargo-containing tubules that are disrupted in *tat-1/chat-1* mutants, thus allowing normal cargo sorting and recycling. We found that loss of DNPP-1 failed to suppress PS appearance on the outer leaflet of plasma membranes or on the luminal side of endomembranes in *tat-1* mutants, and it did not cause obvious changes in the level of PS associated with the cytosolic surface of membranes, as detected by the PS biosensor GFP::Lact-C2. As membrane surface charge and targeting of positively charged proteins in *tat-1* mutants were largely restored by loss of *dnpp-1*, additional mechanisms may be involved to maintain negative surface charge and protein targeting. In addition to PS, highly negatively charged phosphoinositides, such as PIP2 and PIP3, also contribute to the negative surface charge and targeting of proteins with polybasic clusters (Heo *et al.*, 2006). It is possible that loss of DNPP-1 alters the level of membrane PIP2, PIP3, or other negatively charged phospholipids, thus compensating for the loss of membrane PS asymmetry.

Aminopeptidases catalyze the cleavage of amino acids from the amino terminus of substrate proteins or peptides. They play important roles in a variety of biological processes by regulating protein maturation, metabolism, and peptide signaling (Taylor, 1993). DNPP-1 belongs to an evolutionarily conserved family of soluble aspartyl aminopeptidases (DAP), the physiological substrates and biological functions of which are poorly understood, except for their involvement in angiotensin peptide metabolism (Sim *et al.*, 1994; Chen *et al.*, 2012). We found that DNPP-1 possesses aspartyl aminopeptidase activity in vitro, which is required for its cell-autonomous role in endocytic transport in vivo. Like other aminopeptidases, DNPP-1 may regulate the metabolism of its substrates (proteins or peptides), which are involved in endocytic trafficking. Alternatively, cleavage by DNPP-1 may lead to activation or inactivation of target peptides, thereby affecting downstream processes (Hersh *et al.*, 1987; Cadel *et al.*, 1995). *dnpp-1(qx49)* single mutants do not show obvious defects in sorting and recycling but contain aggregated RAB-7–positive vesicles and fewer and smaller gut granules, suggesting a defect in the degradative pathway. Consistent with this, loss of DNPP-1 enhanced rather than suppressed the cargo degradation defect in *tat-1* mutants. The opposing effects of loss of DNPP-1 on endocytic sorting/recycling and degradation suggest that DNPP-1 may participate in multiple steps of endocytic transport by targeting distinct substrates.

We observed that cargoes internalized by either clathrin-dependent or clathrin-independent pathways were efficiently recycled back to plasma membranes in *dnpp-1(qx49) tat-1(qx30)* double mutants, suggesting that the reversion likely occurs at the level of sorting endosomes. Consistent with this, the cargo-containing tubules reappear and can reach RME-1–positive recycling endosomes in *dnpp-1 tat-1* mutants, a process that requires normal functions of RAB-5 and RAB-10. We observed that the number of RME-1–positive endosomes in the basolateral membrane area was not restored to the wild-type level, and RME-1 was absent from some cargo-containing vesicles in *dnpp-1 tat-1* double mutants (Figure 5, R–R″, arrowheads). As cargo recycling was efficiently restored in these worms, additional mechanisms may be involved to deliver cargo to plasma membranes.

MATERIALS AND METHODS
C. elegans strains
Strains of *C. elegans* were cultured and maintained using standard protocols. The N2 Bristol strain was used as the wild-type strain, except for polymorphism mapping, which used Hawaiian strain CB4856. Mutations used in this study are listed below. Linkage group I (LGI): *rab-10(dx2)*. LGIII: *tat-1(qx30)*, *tat-1(tm3110)*, *dnpp-1(qx49)*,

dnpp-1(tm4588). LGIV: chat-1(qx36). LGV: rme-1(b1045). LGX: lmp-1(nr2045). pwIs216 (P_{vha-6}mRFP::RME-1), pwIs112 (P_{vha-6}hTAC::GFP), and pwIs717 (P_{vha-6}hTfR(short)::GFP) were kindly provided by Barth Grant (Rutgers University, Piscataway, NJ). bIs1 (VIT-2::GFP) (Grant and Hirsh, 1999), qxEx1736 (P_{hsp}ssGFP::Lact-C2), qxEx1398 (P_{myo-3}ssGFP::Lact-C2), qxIs154 (P_{unc-122}GFP::Lact-C2), qxEx2247 (P_{vha-6}GLUT-1::GFP), qxEx2841 (P_{vha-6}GFP::RAB-5), qxEx2616 (P_{vha-6}GFP::RAB-7), and qxEx1219 (P_{ges-1}GFP::RAB-10), were used in our previous study (Chen et al., 2010).

Other strains carrying integrated or transgenic arrays used in this study are as follows: qxIs323 (P_{dnpp-1}DNPP-1::mCHERRY), qxIs287 (P_{vha-6}GFP::8+), qxEx1967 (P_{vha-6}GFP::6+), qxEx1970 (P_{vha-6}GFP::4+), qxEx1863 (P_{vha-6}GFP::2+), and qxEx2881 (P_{vha-6}GFP::RAS-2).

Isolation, mapping, and cloning of dnpp-1

qx49 was isolated from a forward genetic screen for mutations that suppress the intestinal vacuoles in tat-1(qx30) mutants. qx49 was mapped to linkage group III and single-nucleotide polymorphism (SNP) mapping was then performed to locate qx49 to a small genetic interval between −1.47 (snp_pkP3099) and −0.75 (snp_F56C9(1)). Transformation rescue experiments were performed, and one fosmid clone in this region, WRM0617aH07, rescued the qx49 phenotype. Long PCR fragments covering different open reading frames within this fosmid clone were tested; only the fragment containing F01F1.9 possessed rescuing ability. F01F1.9 encodes the homologue of the mammalian aspartyl aminopeptidase DNPP-1, which contains 470 amino acids. Sequencing of the dnpp-1 locus in the qx49 mutant identified a G-to-A transition, which resulted in substitution of Glu-331 by Lys. The deletion mutant of dnpp-1, tm4588, contains a 313–base pair deletion and an 8–base pair insertion that removes part of intron 2 and exon 3 of the dnpp-1 gene. A similar suppression phenotype was observed in tm4588 mutants or when dnpp-1 was inactivated by RNAi, suggesting that qx49 is likely a strong loss-of-function or null mutation of dnpp-1.

RNAi

To inactivate dnpp-1, chat-1 or lmp-1 by RNAi, we injected double-stranded RNA synthesized in vitro (~1100 ng/μl) into the gonads of young adult hermaphrodites. Embryos laid between 12 and 20 h postinjection were cultured until the L4 larval or young adult stage, when intestinal phenotypes were examined. For rab-5 and rab-10 RNAi, the bacteria feeding protocol was used as described before (Kamath and Ahringer, 2003). For rab-5 RNAi, adult worms were bleached on rab-5 RNAi (I-4J01) plates. L4 or adult worms of the next generation were scored. For rab-10 RNAi, L1 larvae were treated with rab-10 RNAi (I-3G23), and F1 progeny were examined at the adult stage.

Examination of PS asymmetry and yolk accumulation

Examination of PS asymmetry across plasma membranes or endomembranes was performed as described before (Chen et al., 2010). For examination of yolk accumulation in the intestine, L4 larvae were aged for 72 h post-L4/adult molt, and images were taken with the same exposure time.

Quantification of the distribution of recycling cargo markers

Quantifications of intracellular accumulation of recycling cargoes (hTfR::GFP, hTAC::GFP, GLUT-1::GFP), Lysotracker Red–positive granules, mRFP::RME-1–positive vesicles, and GFP::RAB-10–labeled aggregated structures were performed as described before (Chen et al., 2010). The mRFP::RME-1–labeled aggregated structures were scored within a unit area of 500 μm². Five different regions were chosen for each animal, and eight worms were quantified. The

average total intensity per unit area of GFP::RAB-5 or GFP::RAB-7 in the intestine cells was measured using Image J 1.42q software as described before (Chen et al., 2010). AxioVision Rel. 4.7 software (Carl Zeiss, Jena, Germany) was used to quantify average total intensity per unit area of VIT-2::GFP in fourfold embryos and in the intestine of aged adults (72 h post-L4) as described before (Chen et al., 2010). The colocalization of GFP::RAB-5 and mCHERRY::RAB-7 or GFP::RAB-10 and mRFP::RME-1 was quantified by counting the number of overlapping puncta or aggregates observed within a unit area of 400 μm². Five different regions were chosen for each animal, and six worms were quantified. The total average intensity of GFP::Lact-C2 or charge probes GFP::8+, GFP::6+, and GFP::4+ on plasma membranes and endomembranes in coelomocytes (GFP::Lact-C2) or apical membranes of intestine cells (charge probes) was quantified using Image J 1.42q software. Five different points on each membrane were chosen for each animal, and six animals were scored in each strain.

Statistical analysis

The standard error of the mean (SEM) was used as the y error bar for bar charts plotted from the mean value of the data. Data derived from different genetic backgrounds were compared using Student's two-tailed unpaired t test. Data were considered statistically different with $p < 0.05$ (indicated in the figure legends).

Microscopy and imaging analysis

Differential interference contrast (DIC) and fluorescent images were captured with a Zeiss AxioImager A1 equipped with epifluorescence and an AxioCam monochrome digital camera and were processed and viewed using AxioVision Rel. 4.7 software (Carl Zeiss, Jena, Germany). A 100× Plan-Neofluar objective (numerical aperture 1.30) was used with Immersol 518F oil (Carl Zeiss). For confocal images, a Zeiss LSM 510 Pascal inverted confocal microscope with 488 and 543 lasers was used, and images were processed and viewed using LSM Image Browser software (Carl Zeiss).

Plasmid construction

P_{dnpp-1}dnpp-1::mcherry and P_{dnpp-1}dnpp-1::Flag were constructed by ligating dnpp-1 genomic DNA containing 2.1 kbp of the promoter sequence to pPD49.26-mcherry2 or pPD49.26 through the sites BamHI/NheI and BamHI/KpnI, respectively. For generation of cationic biosensor constructs, DNA fragments of 8+, 6+, 4+, and 2+ were PCR-amplified from EK (EGFP::K-ras4B), EK_{AQ}, EK_{AQ}(K2Q), and EK(K6Q), respectively, and cloned into P_{vha-6}gfp1 through the KpnI site. For construction of markers for specific expression in the intestine, a genomic fragment of dnpp-1 (C-terminal fusion with Flag or ncherry) and ras-2 cDNA were PCR-amplified and cloned into pPD49.26-P_{vha-6}, P_{vha-6}ncherry2 or P_{vha-6}gfp1 through the NheI/KpnI (dnpp-1::Flag), NheI (dnpp-1::ncherry), and KpnI (ras-2) sites. For creating the P_{dnpp-1}dnpp-1(M3)::mcherry construct, point mutations (H92F, H166F, H437F) were introduced by site-directed mutagenesis (QuikChange; Stratagene, Santa Clara, CA) into P_{dnpp-1}dnpp-1::mcherry. For protein expression vectors, dnpp-1 (full-length cDNA) was cloned into pET21b through the sites NheI/HindIII. Point mutations were introduced by a similar strategy described above to generate pET21b-dnpp-1(M3) and pET21b-dnpp-1(E331K). P_{myo-3}dnpp-1::nCherry plasmid was constructed by cloning the 2.4-kbp promoter fragment of myo-3 to pPD49.26 through the BamHI/NheI site; this was followed by ligating DNPP-1::nCherry through the NheI and KpnI sites.

Expression and purification of DNPP-1-His₆

DNPP-1, DNPP-1(M3), or DNPP-1(E331K) tagged with the six histidine residues (DNPP-1-His₆, DNPP-1(M3)-His₆, or DNPP-1(E331K)-His₆)

were expressed in and purified from *Escherichia coli* strain BL21 using an Ni-NTA–agarose column. Purified protein was dialyzed against PBS for 12 h. Protein concentration was determined using the Bio-Rad DC protein assay with bovine serum albumin as the standard protein (Hercules, CA).

Measurement of enzymatic activity

Aminopeptidase activity was determined as previously described by measuring the release of the fluorogenic leaving group, 7-amino-4-methyl-coumarin (NHMec), from the fluorogenic peptide substrates H-Asp-NHMec and H-Glu-NHMec (Bachem, Bubendorf, Switzerland) (McGowan *et al.*, 2009). Fluorescence was detected by using a microplate reader (Paradigm Detection Platform; Beckman Coulter, Brea, CA), with excitation at 360 nm and emission at 465 nm. Enzyme (5 µg) was added to 50 mM Tris-HCl (pH 7.5) buffer; this was followed by the addition of 10 µM substrate. Initial rates were obtained at 37°C over a range of substrate concentrations spanning K_m values of 0.2–50 µM at fixed enzyme concentrations in 50 mM Tris-HCl (pH 7.5). K_m and V_{max} values were obtained from Michaelis-Menten curves with Prism software (GraphPad, La Jolla, CA). Each determination was conducted using seven or eight concentrations of substrate, and each measurement was performed in triplicate. k_{cat} was calculated using a monomer molecular weight of 51,156.

Inhibition of DNPP-1 activity by peptidase inhibitors was performed by preincubating the enzyme with the ion chelators EDTA or *o*-phenanthroline in 50 mM Tris-HCl (pH 7.5, 20 min, 37°C); this was followed by the addition of substrates.

REFERENCES

Babbey CM, Ahktar N, Wang E, Chen CC, Grant BD, Dunn KW (2006). Rab10 regulates membrane transport through early endosomes of polarized Madin-Darby canine kidney cells. Mol Biol Cell 17, 3156–3175.

Cadel S, Pierotti AR, Foulon T, Creminon C, Barre N, Segretain D, Cohen P (1995). Aminopeptidase-B in the rat testes: isolation, functional properties and cellular localization in the seminiferous tubules. Mol Cell Endocrinol 110, 149–160.

Chen B, Jiang Y, Zeng S, Yan J, Li X, Zhang Y, Zou W, Wang X (2010). Endocytic sorting and recycling require membrane phosphatidylserine asymmetry maintained by TAT-1/CHAT-1. PLoS Genet 6, e1001235.

Chen CC, Schweinsberg PJ, Vashist S, Mareiniss DP, Lambie EJ, Grant BD (2006). RAB-10 is required for endocytic recycling in the *Caenorhabditis elegans* intestine. Mol Biol Cell 17, 1286–1297.

Chen Y, Farquhar ER, Chance MR, Palczewski K, Kiser PD (2012). Insights into substrate specificity and metal activation of mammalian tetrahedral aspartyl aminopeptidase. J Biol Chem 287, 13356–13370.

Darland-Ransom M, Wang X, Sun CL, Mapes J, Gengyo-Ando K, Mitani S, Xue D (2008). Role of *C. elegans* TAT-1 protein in maintaining plasma membrane phosphatidylserine asymmetry. Science 320, 528–531.

Daumke O, Lundmark R, Vallis Y, Martens S, Butler PJ, McMahon HT (2007). Architectural and mechanistic insights into an EHD ATPase involved in membrane remodelling. Nature 449, 923–927.

Grant B, Hirsh D (1999). Receptor-mediated endocytosis in the *Caenorhabditis elegans* oocyte. Mol Biol Cell 10, 4311–4326.

Grant B, Zhang Y, Paupard MC, Lin SX, Hall DH, Hirsh D (2001). Evidence that RME-1, a conserved *C. elegans* EH-domain protein, functions in endocytic recycling. Nat Cell Biol 3, 573–579.

Grant BD, Caplan S (2008). Mechanisms of EHD/RME-1 protein function in endocytic transport. Traffic 9, 2043–2052.

Grant BD, Donaldson JG (2009). Pathways and mechanisms of endocytic recycling. Nat Rev Mol Cell Biol 10, 597–608.

Gruenberg J (2001). The endocytic pathway: a mosaic of domains. Nat Rev Mol Cell Biol 2, 721–730.

Harford J, Bridges K, Ashwell G, Klausner RD (1983). Intracellular dissociation of receptor-bound asialoglycoproteins in cultured hepatocytes. A pH-mediated nonlysosomal event. J Biol Chem 258, 3191–3197.

Heo WD, Inoue T, Park WS, Kim ML, Park BO, Wandless T, Meyer T (2006). PI(3,4,5)P3 and PI(4,5)P2 lipids target proteins with polybasic clusters to the plasma membrane. Science 314, 1458–1461.

Hersh LB, Aboukhair N, Watson S (1987). Immunohistochemical localization of aminopeptidase M in rat brain and periphery: relationship of enzyme localization and enkephalin metabolism. Peptides 8, 523–532.

Jovic M, Sharma M, Rahajeng J, Caplan S (2010). The early endosome: a busy sorting station for proteins at the crossroads. Histol Histopathol 25, 99–112.

Kamath RS, Ahringer J (2003). Genome-wide RNAi screening in *Caenorhabditis elegans*. Methods 30, 313–321.

Kelly JA, Neidle EL, Neidle A (1983). An aminopeptidase from mouse brain cytosol that cleaves N-terminal acidic amino acid residues. J Neurochem 40, 1727–1734.

Kostich M, Fire A, Fambrough DM (2000). Identification and molecular-genetic characterization of a LAMP/CD68-like protein from *Caenorhabditis elegans*. J Cell Sci 113, 2595–2606.

Maxfield FR, McGraw TE (2004). Endocytic recycling. Nat Rev Mol Cell Biol 5, 121–132.

McGowan S *et al.* (2009). Structural basis for the inhibition of the essential *Plasmodium falciparum* M1 neutral aminopeptidase. Proc Natl Acad Sci USA 106, 2537–2542.

McLaughlin S, Murray D (2005). Plasma membrane phosphoinositide organization by protein electrostatics. Nature 438, 605–611.

McMahon HT, Gallop JL (2005). Membrane curvature and mechanisms of dynamic cell membrane remodelling. Nature 438, 590–596.

Mukherjee S, Ghosh RN, Maxfield FR (1997). Endocytosis. Physiol Rev 77, 759–803.

Nilsson L, Conradt B, Ruaud AF, Chen CC, Hatzold J, Bessereau JL, Grant BD, Tuck S (2008). *Caenorhabditis elegans* num-1 negatively regulates endocytic recycling. Genetics 179, 375–387.

Nilsson L, Jonsson E, Tuck S (2011). *Caenorhabditis elegans* numb inhibits endocytic recycling by binding TAT-1 aminophospholipid translocase. Traffic 12, 1839–1849.

Pant S, Sharma M, Patel K, Caplan S, Carr CM, Grant BD (2009). AMPH-1/Amphiphysin/Bin1 functions with RME-1/Ehd1 in endocytic recycling. Nat Cell Biol 11, 1399–1410.

Roy MO, Leventis R, Silvius JR (2000). Mutational and biochemical analysis of plasma membrane targeting mediated by the farnesylated, polybasic carboxy terminus of K-ras4B. Biochemistry 39, 8298–8307.

Ruaud AF, Nilsson L, Richard F, Larsen MK, Bessereau JL, Tuck S (2009). The *C. elegans* P4-ATPase TAT-1 regulates lysosome biogenesis and endocytosis. Traffic 10, 88–100.

Sano H, Eguez L, Teruel MN, Fukuda M, Chuang TD, Chavez JA, Lienhard GE, McGraw TE (2007). Rab10, a target of the AS160 Rab GAP, is required for insulin-stimulated translocation of GLUT4 to the adipocyte plasma membrane. Cell Metab 5, 293–303.

Shi A, Liu O, Koenig S, Banerjee R, Chen CC, Eimer S, Grant BD (2012). RAB-10-GTPase-mediated regulation of endosomal phosphatidylinositol-4,5-bisphosphate. Proc Natl Acad Sci USA 109, E2306–E2315.

Sim MK, Choo MH, Qiu XS (1994). Degradation of angiotensin I to [des-Asp1]angiotensin I by a novel aminopeptidase in the rat hypothalamus. Biochem Pharmacol 48, 1043–1046.

Sune A, Bienvenue A (1988). Relationship between the transverse distribution of phospholipids in plasma membrane and shape change of human platelets. Biochemistry 27, 6794–6800.

Taylor A (1993). Aminopeptidases: structure and function. FASEB J 7, 290–298.

Wilk S, Wilk E, Magnusson RP (1998). Purification, characterization, and cloning of a cytosolic aspartyl aminopeptidase. J Biol Chem 273, 15961–15970.

Wilk S, Wilk E, Magnusson RP (2002). Identification of histidine residues important in the catalysis and structure of aspartyl aminopeptidase. Arch Biochem Biophys 407, 176–183.

Yeung T, Gilbert GE, Shi J, Silvius J, Kapus A, Grinstein S (2008). Membrane phosphatidylserine regulates surface charge and protein localization. Science 319, 210–213.